Electromechanical effects in electron structure for GaN/AlN quantum dots

Journal of Physics: Conference Series **107** (2008) 012008 doi:10.1088/1742-6596/107/1/012008

Electromechanical effects in electron structure for GaN/AlN quantum dots

B. Lassen[1], M. Willatzen[1], D. Barettin[1], R. V. N. Melnik[2] and L. C. Lew Yan Voon[3]

[1] The Mads Clausen Institute, The University of Southern Denmark, Denmark
[2] Wilfrid Laurier University, Ontario, Canada
[3] Department of Physics, Wright State University, Ohio, USA

Abstract. We study the impact of using the fully coupled electromechanical equations including piezoelectric effect and spontaneous polarization as compared to the semi-coupled approach, where the strain is solved first without piezoelectric coupling and then inserted into the equation for the electric potential. We show that for circular GaN/AlN quantum dots the fully coupled approach is needed for dots with a radius comparable to or larger than the height, however, when the radius is smaller than the height the semi-coupled approach is sufficient. We highlight this by studying the effect on the electronic structure using an effective mass approximation.

1. Introduction

It is well known that strain due to lattice mismatch in nanoscale semiconductor heterostructures gives important contributions to electronic properties, e.g., it has been shown by O'Reilly et al. [1] how to use strain to minimize the effective mass at the valence-band edge in quantum wells. In the past decade, the impact of piezoelectric effects on the near-bandgap electronic structure and the influence of piezoelectricity and spontaneous polarization on the strain fields and the electric potential has been examined [2, 3, 4, 5, 6, 7]. One of the key questions has been whether it is reasonable to use a semi-coupled model where the strain due to lattice mismatch is calculated first without coupling to the electric field and then inserted into the equation for the electric displacement field. It turns out that the semi-coupled model is adequate for some materials (e.g. InGaN/GaN) but fails for other materials (e.g. AlN/GaN) [7]. Furthermore, results indicate that for a AlN/GaN heterostructure, the spontaneous polarization is just as important as the piezoelectric effect.

In this work we study the influence of the semi-coupled versus the fully-coupled approach on the electronic structure of GaN/AlN quantum dots. Indeed, our work can be viewed as an extension of the earlier work of Andreev and O'Reilly, where they also studied the electronic structure of GaN/AlN quantum dots but only using the semi-coupled model [8]. We employ the wurtzite one-band model for the lower conduction-band structure [5]. We assume that the dot is cylindrical symmetric around the c-axis. Although wurtzite quantum dots are usually found with a hexagonal pyramidal structure we do not expect to find major differences between hexagonal and cylindrical symmetric structures. This has recently been asserted for wurtzite nanowires [9]. Due to the fact that the $k \cdot p$ model and the system of coupled equations for the

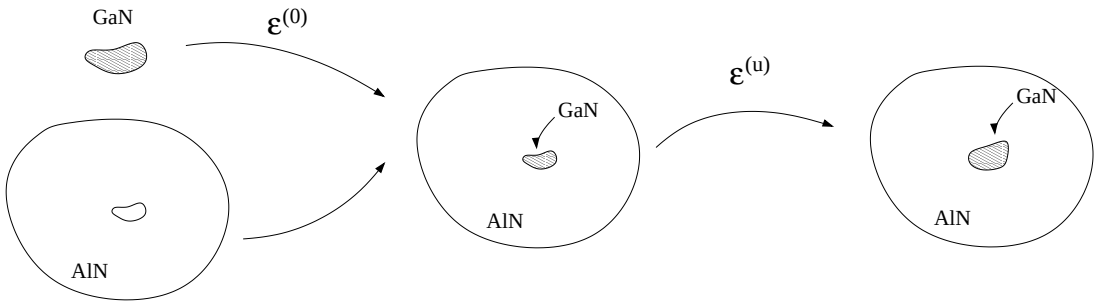

Figure 1. Schematic picture of conceptual shrink fit procedure.

strain and the electric fields are cylindrical symmetric around this axis [10, 11] the cylindrical geometry enables us to reduce the complete model to a two-dimensional problem.

The paper is organized as follows. In section 2 we introduce the governing equations for the electromechanical part and the electronic structure. In section 3 we present results found using the semi-coupled and the fully-coupled approaches for circular GaN/AlN quantum dots with varying radius and highlight the difference. And finally in section 4 we give concluding remarks.

2. Theory

The system under consideration is an embedded GaN quantum dot surrounded by a AlN barrier, see figure 1. Due to differences in properties of the two materials there will be an intrinsic electric field and strains in the system even in the equilibrium configuration. The driving mechanisms behind this are the differences in lattice constants and the spontaneous polarizations of the two materials. In this work we disregard all dislocations in the system, i.e., we assume that the system has been pseudomorphically grown. Pseudomorphically grown low-dimensional structures are modeled by assuming that the system has been prepared by the shrink fit method, i.e., conceptually we assume that the dot material was shrunk or expanded so as to fit the lattice constant to the barrier material. The resulting system is not in equilibrium and as a result the system will relax until it reaches equilibrium, see figure 1. AlN and GaN are piezoelectric so in the modeling of the relaxation we need to take into account the coupling between the electric field and the strain tensor. In this work we study two different electromechanical continuous approaches, the fully-coupled and the semi-coupled approaches. Theses approaches are explained in the following.

2.1. The Fully-Coupled Approach

The linear constitutive relations for stress and electric displacement for any material are given by:

$$\sigma_{ik} = C_{iklm}\varepsilon_{lm} + e_{nik}\partial_n V, \tag{1}$$

and

$$D_i = e_{ilm}\varepsilon_{lm} - \epsilon_{in}\partial_n V + P_i^{sp}, \tag{2}$$

where C_{iklm}, e_{nik}, ϵ_{in}, ε_{lm}, V, and P^{sp} are the constants of elastic moduli, the piezoelectric constants, the permittivity, the strain tensor, the electrical potential, and the spontaneous polarization, respectively. Here, and in the following, ∂_n denote the derivative along direction n. Including only linear deformation gradient terms, i.e., first order in $\partial_i u_j$, where $\mathbf{u}$ is the displacement vector, the strain is given by:

$$\varepsilon_{ij} = \varepsilon_{ij}^{(0)} + \varepsilon_{ij}^{(u)}, \tag{3}$$

where $\varepsilon_{ij}^{(0)}$ is the strain from the shrink fit (lattice mismatch) and

$$\varepsilon_{ij}^{(u)} = \frac{1}{2}(\partial_j u_i + \partial_i u_j), \tag{4}$$

is the strain from the relaxation. Here u_i is the displacement of the middle configuration in figure 1. In literature, a different definition of the lattice mismatch is often used which results in a minus sign in front of $\varepsilon_{ij}^{(0)}$ in equation (3), see for example [5]. The two definitions can be shown to be equivalent to first order in the lattice mismatch.

The electromechanical equations of equilibrium are Navier's equations:

$$\partial_j \sigma_{ij} = 0, \tag{5}$$

and the Poisson equation:

$$\partial_i D_i = 0, \tag{6}$$

where we for simplicity assume that there are no external charges in the system. These together with the constitutive relations result in four second order partial-differential equations in the four unknowns u_1, u_2, u_3 and V.

2.2. The Semi-Coupled approach

In the semi-coupled approach the equations for strain are solved first without any coupling to the electric field, i.e., we solve

$$\sigma_{ik} = C_{iklm}\varepsilon_{lm}, \tag{7}$$

and

$$\partial_j \sigma_{ij} = 0,$$

for the displacement components u_1, u_2, u_3. These are then used as input to the electric displacement vector:

$$D_i = e_{ilm}\varepsilon_{lm} - \epsilon_{in}\partial_n V + P_i^{sp}, \tag{8}$$

after which Poisson's equation:

$$\partial_i D_i = 0,$$

is solved for the electric potential V. This corresponds to setting e equal to zero in the constitutive relation for the stress but keeping it in the constitutive relation of the electric displacement. That is we take into account only half of the piezoelectric effect.

2.3. Wurtzite Structure

In the following we consider wurtzite GaN in AlN quantum dots. Using the symmetries of wurtzite the non-zero material parameters can be reduced to the set given below (x_3 is directed along the c-axis and x_1 and x_2 perpendicular to the c-axis):

$$\begin{aligned}
&C_{1111} \equiv C_{11}; \quad C_{1122} \equiv C_{12}; \quad C_{1133} \equiv C_{13};\\
&C_{3333} \equiv C_{33}; \quad C_{2323} \equiv C_{44}; \quad C_{2121} \equiv (C_{11} - C_{12})/2;\\
&e_{311} \equiv e_{31}; \quad e_{333} \equiv e_{33}; \quad e_{113} \equiv e_{15};\\
&\epsilon_{11} \equiv \epsilon_{\perp}; \quad \epsilon_{22} \equiv \epsilon_{\perp}; \quad \epsilon_{33} \equiv \epsilon_{||};
\end{aligned}$$

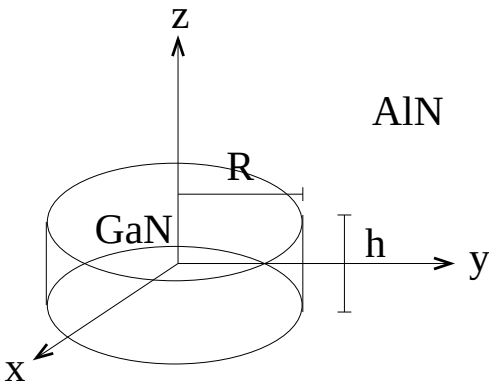

Figure 2. Geometry of the quantum dot under consideration. R is the radius of the dot and h is the height.

and the lattice mismatch is given by:

$$\varepsilon_{ij}^{(0)} = (\delta_{ij} - \delta_{i3}\delta_{j3})a(\mathbf{r}) + \delta_{i3}\delta_{j3}c(\mathbf{r}). \tag{9}$$

where

$$a(\mathbf{r}) = \frac{a_{matrix} - a_{QD}}{a_{matrix}}, \qquad c(\mathbf{r}) = \frac{c_{matrix} - c_{QD}}{c_{matrix}}, \tag{10}$$

in the dot and zero otherwise. The spontaneous polarization in wurtzite is directed along the c-axis, so:

$$P_1^{sp} = P_2^{sp} = 0, \text{ and } P_z^{sp} = P_{sp}.$$

In the rest of the paper we use the notation $x_1 = x$, $x_2 = y$ and $x_3 = z$.

2.4. System

It can be shown that both the fully-coupled and the semi-coupled models are invariant under rotation about the c-axis [11]. In order to exploit this symmetry fully and because we are not, in this work, interested in the exact heterostructure geometry, we assume that the dot is cylindrical symmetric around the c-axis. Furthermore, we use the simplest cylindrical symmetric structure which is a cylinder, see figure 2. In order to take advantage of rotation invariance, we transform the governing equations to cylindrical coordinates, reduce it to a two dimensional problem and solve the resulting equations using the finite element method (using ComSol multiphysics). See the paper by Barettin et al. [11] for a more details. The values of the material parameters are taken from Fonoberov and Balandin [5] and listed in table 1.

2.5. Electronic Structure - k·p Theory

For the electronic structure part we use the k·p one-band model (effective mass approximation) for the conduction band. The one-band Hamiltonian for wurtzite including the effects of strain and electric field is given by:

$$H = \left(k_z \frac{\hbar^2}{m_e^{||}} k_z + k^{\perp} \frac{\hbar^2}{m_e^{\perp}} k^{\perp} \right) + V_{edge} + a_c^{||}\varepsilon_{zz} + a_c^{\perp}\left[\varepsilon_{xx} + \varepsilon_{yy}\right] - eV, \tag{11}$$

where $m_e^{||}$ and $m_e^{\perp}$ are effective masses, $a_c^{||}$ and $a_c^{\perp}$ are deformation potentials, e is the electron charge, $k_z = -i\partial_z$,

$$k^{\perp} = -i \begin{pmatrix} \partial_x \\ \partial_y \end{pmatrix}, \tag{12}$$

and V_{edge} is the band-edge potential of the heterostructure. It is instructive to think of the electron as being a particle moving in the effective potential:

$$V_{eff} = V_{edge} + a_c^{||}\varepsilon_{zz} + a_c^{\perp}\left[\varepsilon_{xx} + \varepsilon_{yy}\right] - eV, \tag{13}$$

as this carries all the information about the influence of the electromechanical fields. The material parameters used in this paper are taken from the paper by Fonoberov and Balandin [5] and are given in table 2.

3. Results

3.1. Electromechanical

In figure 3, we show ε_{zz} as a function of z at $(x, y) = (0, 0)$ based on the fully-coupled (solid lines) and the semi-coupled (dashed lines) models for different R values at constant height $h = 3$ nm. For both models we see that the strain inside the dot decreases as the radius is increased and it goes from having a pronounced position dependence to being almost constant inside the dot. This is due to two competing effects. The first is a confinement effect due to the presence of the barrier material at the sides of the quantum dot. The second is the Poisson effect due to the confinement in the (x, y) plane. As long as the aspect ratio (R/h) is close to 1, the confinement in the z-direction is more pronounced than the Poisson effect, however, as the aspect ratio is increased the Poisson effect gradually wins over the confinement effect. We also note that the electric field and the strain in the large aspect ratio limit approaches results for the quantum well (1D) case [7]. Comparing the two models we see that for small R the difference is negligible, whereas for large R there is a noticeable difference. To understand why this is the case we plot in the sub-figure of figure 3b the electric field. Here we see that for small R the electric field is relatively small and as a result giving a small additional contribution to the strain part. However, as the radius is increased, the electric field also increases resulting in

	a	c	C_{11}	C_{12}	C_{13}	C_{33}	C_{44}	e_{15}	e_{31}	e_{33}	P_{sp}	$\epsilon^{||}$	$\epsilon^{\perp}$
GaN	3.189	5.185	390	145	106	398	105	−0.49	−0.49	0.73	−0.029	10.01	9.28
AlN	3.112	4.982	396	137	108	373	116	−0.60	−0.60	1.46	−0.081	8.57	8.67

Table 1. Material parameters for GaN and AlN. Values are taken from [5]. Lattice constants are in Å, elastic moduli in GPa, piezoelectric constants in C/m^2 and permittivities are given relative to the vacuum permittivity.

	$m_e^{||}$ $[m_0]$	$m_e^{\perp}$ $[m_0]$	V_{edge} $[eV]$	$a_c^{||}$ $[eV]$	$a_c^{\perp}$ $[eV]$
GaN	0.2	0.2	0	−9.5	−8.2
AlN	0.28	0.32	1.955	−12.0	−5.4

Table 2. Material parameters appearing in the one-band Hamiltonian [equation (11)]. Values are taken from [5]. m_0 is the free electron mass.

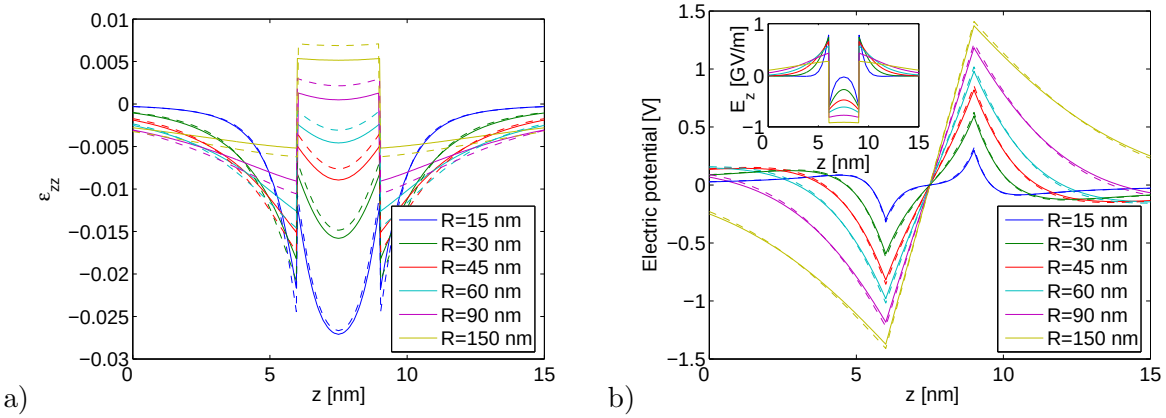

Figure 3. The strain element ε_{zz} (a) and the electric potential V (b) as a function of z at $(x, y) = (0, 0)$ nm for different R values. The solid (dashed) lines are results of the fully-coupled (semi-coupled) model. The insert in figure b shows the electric field in the z direction ($E_z = -\partial_z V$).

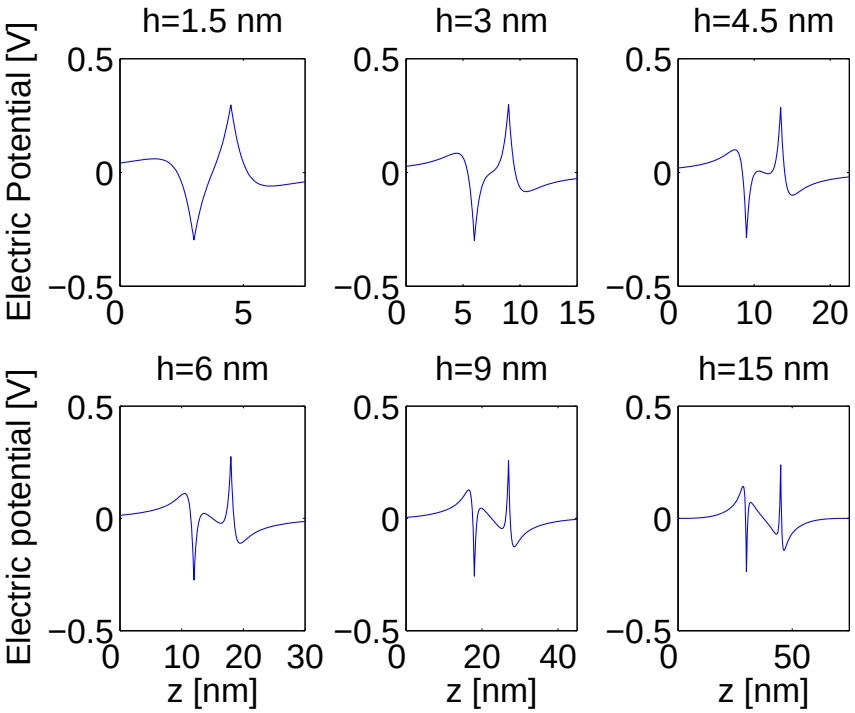

Figure 4. The electric potential V as a function of z at $(x, y) = (0, 0)$ nm for different h values and radius $R = 1.5$ nm found using the fully-coupled model.

a larger piezoelectric coupling and a larger difference between the semi-coupled and the fully-coupled models. Our results are in excellent agreement with results in the paper by Andreev and O'Reilly [8].

In figure 4 we show the electric potential for different heights and with fixed radius ($R = 1.5$ nm). We only show results of the fully-coupled model because the two models give more or less the same results. As the height of the dot is increased something rather unexpected

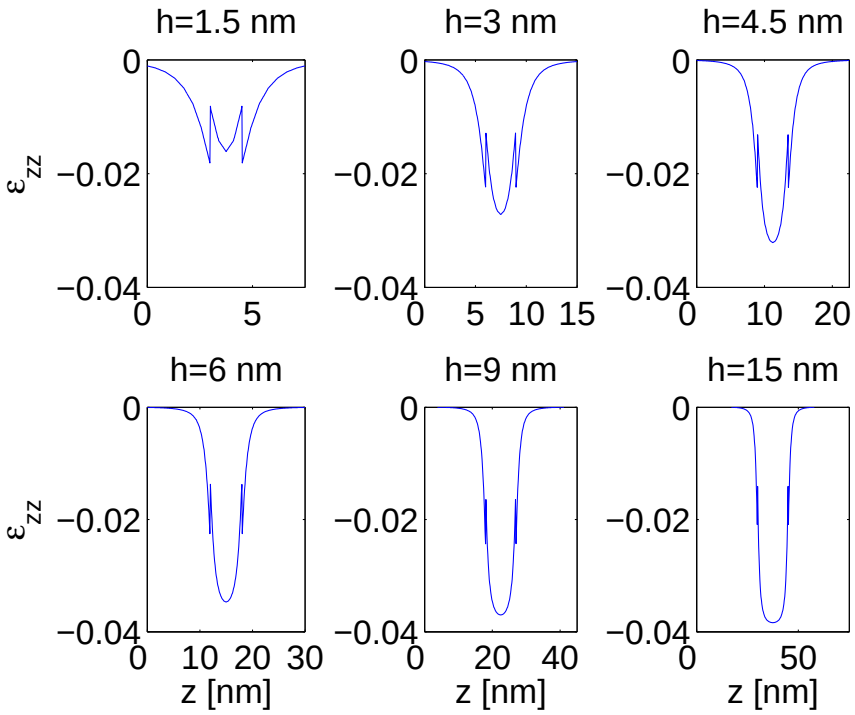

Figure 5. The strain component ε_{zz} as a function of z at $(x, y) = (0, 0)$ nm for different h values and radius $R = 1.5$ nm.

happens. Around a height of 4.5 nm the electric potential inside the dot changes form having a positive slope to having a negative slope, i.e., the electric field in the z-direction goes from being negative to being positive. However, close to the interface the sign of the slope does not change and only the magnitude changes somewhat. The reason for this behavior can be traced back to the strain tensor. In figure 5 we show the ε_{zz} component of the strain for the same heights and the same radius as in figure 4. Here we see that as the height is increased the magnitude of ε_{zz} increases inside the dot. As a result the effect of the strain on the electric potential increases and at some point it becomes as predominant as (or more predominant than) the spontaneous polarization resulting in the sign changes of the slope.

3.2. Electronic structure

In figure 6 we show the first four conduction-band energies with $F_3 = 1/2$ (the total angular momentum in the z-direction) as a function of the radius. We see the usual decrease in the energies as the radius is increased. For larger radii we see that the groundstate energy goes below the conduction band edge of GaN. This is because of the shape of the electric potential giving the effective potentials shown in figure 7. Similar results have been presented by Fonoberov and Balandin [5]. In the sub-figure of figure 6 we show the difference in the groundstate energy between the semi-coupled and the fully-coupled models. Here, it is seen that for small radii the two models give more or less the same energy, but as the radius is increased the discrepancy grows and levels out at around 36 meV. This is directly related to the observations made in the previous section, where we saw a reduced influence of the full coupling for small dots due to a reduction in the electric field. From this we see that for dots with a large radius it is important to include the full coupling as it give contribution of the same order as the exciton binding energy [12].

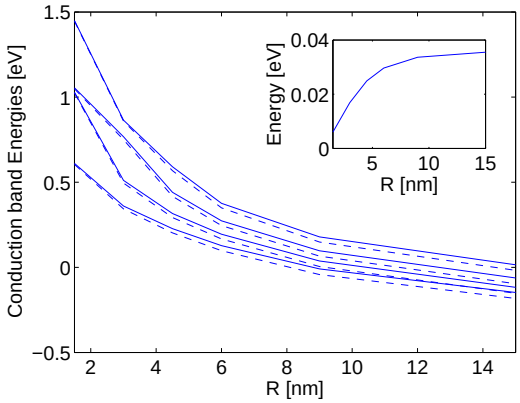

Figure 6. The first four conduction band energies with $F_3 = 1/2$.The solid (dashed) lines are results of the fully-coupled (semi-coupled) model and. The insert shows the difference in the ground-state energy between the fully-coupled and the semi-coupled model.

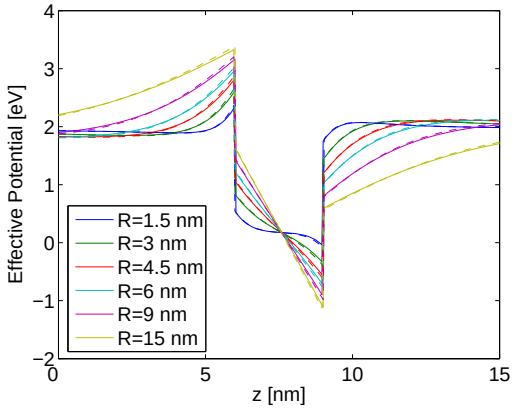

Figure 7. The effective potential V_{eff} as a function of z at $r = 0$ nm for different R values. The solid (dashed) lines are results of the fully-coupled (semi-coupled) model.

4. Conclusion

We have shown that the accuracy of using the semi-coupled approach depends on the shape of cylindrical GaN/AlN quantum dots. For dots with a radius comparable to or larger than the height it is insufficient to use the semi-coupled approach giving an error of up to 36 meV in the energy of the electron which is comparable to exciton binding energies in these structures. However, for dots with a small radius the semi-coupled approach is sufficient.

Furthermore, we have seen that the electric potential (and the strain tensor) is governed by the interplay between both the spontaneous polarization and the strain due to the lattice mismatch and which effect it predominant very much depends on the geometry and the material composition.

Acknowledgements

LYV would like to thank the Research Council at Wright State University for a travel grant.

References

[1] E. P. O'Reilly and G. P. Witchlow. *Phys. Rev. B*, 34, 6030, 1986.
[2] Jin Wang, J. B. Jeon, Yu. M. Sirenko, and K. W. Kim. *IEEE Photonics Technology Letters*, 9, 728, 1997.
[3] E. Pan. *Journal of Applied Physics*, 91, 3785, 2002.
[4] B. Jogai, J. D. Albrecht, and E. Pan. *Journal of Applied Physics*, 94, 3984, 2003.
[5] V. A. Fonoberov and A. A. Balandin. *Journal of Applied Physics*, 94, 7178, 2003.
[6] U. M. E. Christmas, A. D. Andreev, and D. A. Faux. *Journal of Applied Physics*, 98, 073522, 2005.
[7] M. Willatzen, B. Lassen, L. C. Lew Yan Voon, and R. V. N. Melnik. *Journal of Applied Physics*, 100, 024302, 2006
[8] A. D. Andreev, and E. P. O'Reilly. *Physica E*, 10, 553, 2001.
[9] B. Lassen, M. Willatzen, R. Melnik, and L. C. Lew Yan Voon. *Journal of Materials Research*, 21, 2927, 2006.
[10] L. C. Lew Yan Voon, C. Galeriu, B. Lassen, M. Willatzen, and R. Melnik. *Applied Physics Letters*, 87, 041906, 2005.
[11] D. Barettin, B. Lassen and M. Willatzen, Submitted to proceedings of 07w5057 *Physics-Based Mathematical Models of Low-Dimensional Semiconductor Nanostructures: Analysis and Computation*, Banff, Canada, 2007.
[12] P. Ramvall, P. Riblet, S. Nomura, Y. Aoyagi, and S. Tanaka. *Journal of Applied Physics*, 87, 3883, 2000.